Reorganization of the outer layer of a model of the plasma membrane induced by a neuroprotective aminosterol

Reorganization of the outer layer of a model of the plasma membrane induced by a neuroprotective aminosterol

Beatrice Barletti[1]†, Giacomo Lucchesi[1], Stefano Muscat[2], Silvia Errico[3,4], Denise Barbut[5], Andrea Danani[2], Michael Zasloff[5,6], Gianvito Grasso[2], Fabrizio Chiti[3], Gabriella Caminati[1]*

[1]*Department of Chemistry and CSGI, University of Florence, Via della Lastruccia, 3 I – 50019 Sesto Fiorentino, Florence, Italy*

[2]*Dalle Molle Institute for Artificial Intelligence (IDSIA), University of Applied Sciences and Arts of Southern Switzerland (SUPSI), University of Italian Switzerland (USI), Lugano, Switzerland*

[3]*Department of Experimental and Clinical Biomedical Science, University of Florence, Viale G.B. Morgagni, 50 I – 50134 Florence, Italy*

[4]*Centre for Misfolding Diseases, Department of Chemistry, University of Cambridge, Cambridge, UK*

[5]*Enterin Inc., 2005 Market Street, Philadelphia, Pennsylvania 19103, USA*

[6]*MedStar-Georgetown Transplant Institute, Georgetown University School of Medicine, Washington DC, USA*

Corresponding author: gabriella.caminati@unifi.it

DOI:10.1016/j.colsurfb.2022.113115

† Current Address: Institut Max von Laue - Paul Langevin, 71, avenue des Martyrs - CS 20156 - 38042 Grenoble cedex 9 (France)

Abstract

Trodusquemine is an amphipathic aminosterol that has recently shown therapeutic benefit in neurodegenerative diseases altering the binding of misfolded proteins to the cell membrane. To unravel the underlying mechanism, we studied the interactions between Trodusquemine (TRO) and lipid monolayers simulating the outer layer of the plasma membrane. We selected two different compositions of dioleoylphosphatidylcholine (DOPC), sphingomyelin (SM), cholesterol (Chol) and monosialotetrahexosylganglioside (GM1) lipid mixture mimicking either a lipid-raft containing membrane (L_d+S_o phases) or a single-phase disordered membrane (L_d phase). Surface pressure-area isotherms and surface compressional modulus-area combined with Brewster Angle Microscopy (BAM) provided the thermodynamic and morphological information on the lipid monolayer in the presence of increasing amounts of TRO in the monolayer. Experiments revealed that TRO forms stable spreading monolayers at the buffer-air interface where it undergoes multiple reversible phase transitions to bi- and tri-layers at the interface. When TRO was spread at the interface with the lipid mixtures, we found that it distributes in the lipid monolayer for both the selected lipid compositions, but a maximum TRO uptake in the rafts-containing monolayer was observed for a Lipid/TRO molar ratio equal to 3:2. Statistical analysis of BAM images revealed that TRO induces a decrease in the size of the condensed domains, an increase in their number and in the thickness mismatch between the L_d and S_o phase. Experiments and MD simulations converge to indicate that TRO adsorbs preferentially at the border of the S_o domains. Removal of GM1 from the lipid L_d+S_o mixture resulted in an even greater TRO-mediated reduction of the size of the S_o domains suggesting that the presence of GM1 hinders the localization of TRO at the S_o domains boundaries.

Taken together these observations suggest that Trodusquemine influences the organization of lipid rafts within the neuronal membrane in a dose-dependent manner whereas it evenly distributes in disordered expanded phases of the membrane model.

Keywords: Trodusquemine, Neurodegenerations, Lipid Rafts models, Phospholipid monolayers, Plasma membrane

Introduction

Neurodegenerative diseases are a series of pathologies characterized by a progressive and irreversible loss of neurons of the central nervous system [12]. The mechanisms involved in these diseases are very complex and consequently still mostly unknown, but some of these diseases are caused by the conversion of specific peptides or proteins from their native, soluble and intrinsically disordered form into well-defined, insoluble fibrillar aggregates [3,4,5].

Aminosterols have been recently proposed as active protagonists against protein misfolding in neurodegenerations and several studies have highlighted the ability of these molecules to block the neurotoxic effect of α-synuclein and β-amyloid aggregates, known to be among the main causes of the development of Alzheimer's and Parkinson's diseases[6,7,8,9].

Squalamine, a cationic amphipathic aminosterol isolated from the dogfish shark *Squalus acanthias*[10] was extensively studied for its interesting results for the treatment of neurodegeneration associated with α-synuclein [11,12] and has just completed a multicenter, randomized, double-blind, placebo-controlled phase-2b clinical trial in patients with constipation related to Parkinson's disease (KARMET, identifier NCT03781791) and shown improvement in constipation as well as hallucinations and dementia. A previous multicenter, open label phase 2 study in patients with Parkinson's disease (RASMET, identifier NCT03938922) had also shown improvement in constipation, sleep, REM-behavior disorder, hallucinations and dementia[13]. Another multicenter, open label phase 1 study is active on Parkinson's disease cases with dementia (identifier NCT03938922).

Trodusquemine (TRO) is another aminosterol isolated from the dogfish shark *Squalus acanthias*[14] and is structurally very similar to squalamine. TRO has a spermine group, instead of the spermidine group found in squalamine, that imparts a higher positive charge at physiological pH. Previous studies demonstrated that TRO is effective at lower doses [15,16], crosses the blood-brain barrier [17] and can stimulate regeneration of tissues and organs[18]. TRO was proved to slow down the lipid-induced aggregation of α-synuclein and inhibit secondary nucleation of amyloid fibril formation[11], while it was found to accelerate the amyloid fibril formation process of β-amyloid by catalyzing its conversion to more mature fibrils that exhibit lower neurotoxicity [12]. TRO was also found to displace α-synuclein, $A\beta_{42}$ as well as model protein preformed oligomers from the cell membrane in a dose-dependent manner[10,12,19] .In the attempt to establish the mechanism of binding of TRO to the cell membrane, we previously studied the interactions of TRO with reconstituted liposomes in the form of large unilamellar vesicles (LUVs) formed by four natural lipids[20]. The results revealed that TRO changes the membrane physico-chemical properties interfering with the

binding of misfolded protein. In particular, TRO decreased the total negative charge of the lipid bilayer, as determined with ζ-potential measurements, changed the spatial distribution of the constituent lipids, as observed by lipid-lipid FRET experiments, and caused an increment of the mechanical resistance of the lipid membrane to indentation, when probed with atomic force microscopy (AFM) applying a force perpendicular to the bilayer plane.

In the present work we aim to investigate and understand the mechanism of interaction between TRO and a biomimetic model of the outer leaflet of the neuronal cell membrane. Cell membranes are complex assemblies of lipids and proteins that separate the cytosol from the surrounding extracellular environment. For its complexity, the study of real cell membranes is difficult to achieve and to perform a more in-depth study artificial biomimetic models, such as Langmuir monolayers, are commonly used. The mimetic model must be similar enough to the cell membrane, but also simple enough to be accessible by physical measurements[21].

An important issue for the use of artificial biomimetic models is the choice of phospholipids and other lipids, as well as composition ratios that should be as close as possible to those of the real cell membranes. Results on an average idealized mammalian plasma membrane showed that phosphatidylcholines (PC), sphingomyelin (SM), and gangliosides (GM) are predominantly in the outer leaflet whereas phosphatidylethanolamine (PE), phosphatidylserine (PS) and other charged lipids are predominantly in the inner leaflet[22].In this work, we focused on a four-component lipid mixture mimicking the outer leaflet of the neuronal plasma membrane[23,24]and used, therefore, dioleoylphosphatidylcholine (DOPC), sphingomyelin (SM),cholesterol (Chol) and monosialotetrahexosylganglioside (GM1) lipid mixture. We studied two different compositions that, according to the literature[25], mimic a single-phase disordered membrane (L_d) and a two-phase membrane containing both a disordered phase and gel-phase domains that in cells are generally referred to as lipid-rafts (L_d-S_o). In this latter case, the co-existence of domains differing in chemical composition physical properties, creates an optimal environment for protein function and cellular processes, such as trafficking, signal transduction and entry of pathogens[26,27,28,29].

Lipid-rafts play an important role in human physiology and pathogenesis of different diseases, evidence of their crucial roles in neurodegenerative diseases, such as Alzheimer's and Parkinson's diseases, have been extensively described[5,30]. It is in fact increasingly clear that the aggregation processes of proteins or peptides involved in neurodegeneration are accelerated by their binding to the lipid membrane[31,32].

Recent works evidenced that ordered domains extracted from the outer leaflet of the plasma membranes are enriched in anionic glycosphingolipids GMs[33] such as GM1, known to affects neuronal plasticity and repair mechanisms[34]. More importantly, GM1 has been implicated in AD pathology, through

formation of GM1-bound Aβ (G-Aβ) species and it has previously been demonstrated to accelerate aggregation of $A\beta_{1-40}$[35]. More recently, novel insight in the potential pathogenic role of GM1-Aβ interactions was suggested by the G M1-Aβ localization to mature amyloid aggregates associated with neurotoxic plaque formation and AD pathogenesis[36].

Therefore, we studied the mechanism of interaction of TRO with lipid monolayers simulating the outer layer of the plasma membrane by co-spreading TRO with the desired DOPC/SM/Chol/GM1lipid mixture. Surface pressure-area isotherms were used to obtain structural and thermodynamic information of the monolayer systems; the results were combined with a morphological analysis performed through Brewster Angle Microscopy (BAM) that provided the impact of Trodusquemine on the distribution, size, and thickness of the S_o domains, either in the presence or the absence of GM1 in the monolayer.

Materials and Methods

Materials. Trodusquemine ($C_{37}H_{72}N_4O_5S{\cdot}3HCl$, 794.44 g/mol, MSI–1436) was supplied by Enterin, (Philadelphia, USA); 1,2-dioleoyl-sn-glycero-3-phosphocoline ($C_{44}H_{84}NO_8P$, PC 18:1 Δ9-cis, DOPC, 786.113 g/mol, CAS: 4235-95-4), sphingomyelin (egg SM, chicken, 710.965 g/mol, CAS: 383907-87-7), monosialotetrahexosylganglioside 1 (GM1 Ovine Brain, 1568.805 g/mol, CAS: 37758-47-7) were purchased from Avanti Polar Lipids (Alabaster, AL, USA); cholesterol ($C_{27}H_{46}O$, Chol, 386.654 g/mol, CAS: 57-88-5) was purchased from Sigma-Aldrich (Darmstadt, Germany); potassium phosphate monobasic (KH_2PO_4, 136.09 g/mol, CAS: 7778-77-0), potassium phosphate dibasic (K_2HPO_4, 174.18 g/mol, CAS: 7758-11-4), Chloroform ($CHCl_3$, 99%), methanol (CH_3OH, 99%) and dimethyl sulfoxide ($(CH_3)_2SO$, DMSO, 78.13 g/mol, CAS: 67-68-5) were purchased from Honeywell. Ultrapure water (resistivity =18.2 MΩ cm, pH 5.6 at 25 °C) was obtained with a Milli-Q/Simplicity® set-up (Millipore, Italy). The glass containers were washed with chromic acid solution, rinsed with ultrapure water, and flushed with nitrogen. Chemical structures of lipids used for Langmuir monolayer formation are reported in **Figure SI1**.

We prepared monolayers with the two different compositions indicated in the phase diagram[37] reported in **FigureSI1e** that mimic a lipid-raft containing membrane (L_d+S_o) with composition DOPC/SM/Chol/GM1 65:33:1:1 and a single-phase disordered membrane (L_d) with composition DOPC/SM/Chol/GM1 90:8:1:1. Previous studies[15] on such compositions demonstrated that with the addition of a small fraction of GM1 (1%) the lipids partition in L_d and S_o domains.

Langmuir monolayers at liquid-air interface. Two different Langmuir film balances were used to study spreading monolayers at liquid-air interface: a rectangular KSV 3000 Trough (KSV, Finland) equipped with a platinum Wilhelmy plate placed on an anti-vibration table TMC (Technical Manufacturing Corporation, USA) for binary monolayers and TRO on water (supplementary material). Brewster Angle Microscopy experiments were run on a Nima 710 Trough (Nima Technology, England) equipped with a 1 cm wild filter paper Wilhelmy plate (Whatman no. 1 paper) connected to EP3View 2.05 software to study the systems on buffer solution. In all cases the monolayer was spread from a chloroform/methanol 2:1 (vol/vol) solution using Hamilton® microliter syringe ([Lipids]=1 mM, spreading volume 100-150 µL). For the TRO solution a drop of DMSO was added to facilitate the solubilization ([TRO]=1 mM, spreading volume 100 µL). 20 minutes were allowed for solvent evaporation before monolayer compression. All experiments were performed at 20 °C, temperature was controlled by circulating water at a temperature of 20°C ± 0.5 °C, the compression speed was set at 10 mm/min in the case of the KSV 3000 trough and 15 cm^2/min in the case of the Nima set-up. Reported isotherms are the average of at least three independent runs.

Monolayer data analysis

The limiting area (A_0), which represents the area occupied by the polar head of each molecule at maximum packing, was obtained from intersection at π = 0 mN/m of the tangent in the point of higher slope of the isotherm.

The analysis of the excess molecular area as a function of the composition of the mixtures was used to investigate the lateral interactions between components in the monolayer[38,39,40,41]. Experimental surface areas were computed using the average molecular weight of the corresponding mixtures. The experimental surface area at constant surface pressure, A_{mix}, obtained for the mixed monolayer system was compared with the ideal molecular area, A_{id}, calculated through equation 1[42,43]:

$$A_{id} = \chi_1 \cdot A_1 + \chi_2 \cdot A_2 \qquad \text{Eq. 1}$$

Where A_1 and A_2 are the molecular areas of each single component (defined 1 and 2) in their pure films at a given surface pressure and X_1 and X_2 are the molar fractions of the respective component in the mixed film. Comparing the experimental molecular areas, A_{mix}, at constant π with the ideal molecular areas calculated according to equation 1, it is possible to determine whether the interactions are repulsive ($A_{mix}>A_{id}$), attractive ($A_{mix}<A_{id}$) or ideal ($A_{mix}=A_{id}$).

The surface compressional modulus (C_s^{-1}) provides an estimate of the elasticity of the monolayer, C_s^{-1} is determined, at a constant temperature, by the following relationship (Eq.2):

$$C_s^{-1} = -A\left(\frac{d\pi}{dA}\right)_T \qquad \text{Eq. 2}$$

Where A is the molecular area and π is the surface pressure, C_s^{-1} values lower than 50 mN/m identify liquid-expanded phases whereas liquid-condensed monolayer phases show C_s^{-1} in the range 100-250 mN/m. Incipient collapse surface pressure, $\pi_{coll.}$ was determined as the surface pressure at the maximum C_s^{-1}[144].

Crisp-Defay rule[454647] was used to determine whether the lipid mixture, considered as a single lipid component, and TRO were miscible in Langmuir monolayers. Briefly, if the film components are immiscible, then provided the temperature and external pressure remain constant, the surface pressure corresponding to a phase transition (including the surface collapse pressure) will be invariant with monolayer composition.

All surface pressure-area isotherms were analyzed using Igor Pro software from WaveMetrics and A_0, the excess molecular area (A_{mix}), the compression modulus (Cs^{-1}) and incipient collapse pressure, $\pi_{coll.}$, were determined at the following values of surface pressures: 5, 15, 25 mN/m.

Brewster Angle Microscopy (BAM). Brewster Angle Microscopy (BAM) images were recorded during the compression cycle at different surface pressure by means of Imaging Ellipsometer EP3 (Nanofilm Technologies GmbH, Göttingen, Germany) equipped with a 50 mWNd:YAG laser (λ = 532 nm). The experiments were performed around an angle of incidence of 53.15° (Brewster Angle of water) and a laser output of 30 %. The angle was varied between 50.80° e 53.15° to highlight different phases of the monolayer. Analyzer and compensator were set to zero, while the polarizer was varied between 0° and 2° to improve the image contrast. A black glass plate was positioned at the bottom of the trough to avoid scattering of light from the trough inner surface. All experiments were performed using a 10x magnification with a lateral resolution of 2 μm. The images were analyzed by means of ImageJ 1.52a Software (National Institutes of Health, USA) to obtain the size and distribution of the domains, the average area fraction and circularity. The thickness of the domains was estimated following a protocol based on the conversion of the greyscale color code into thickness; similar protocols were previously used also by other authors[48,49].

Molecular dynamics simulations – lipid bilayer

The interaction of TRO molecules with lipid raft was evaluated by molecular dynamics simulations. Five types of molecular systems were investigated: a phospholipid bilayer constituted by 400 lipids and the same bilayer in presence of 1, 2, 3, 4, and 5 TRO molecules, respectively. A fully hydrated lipid bilayer of dibehenoyl-phosphatidylcholine (DBPC) and dilinoleyl-phosphatidylcholine (DIPC) with a mole ratio of 3:1

was created using the bilayer builder insane[50]. DBPC has long saturated chains (22:0), whereas DIPC's are shorter and polyunsaturated (18:2). The gel-to-liquid transition temperature of DBPC and DIPC are 348 K and 216 K respectively (**Figure SI10a**). We have chosen DBPC and DIPC as lipids components of a toy model membrane because have gel-to-liquid transition temperature well separated, accelerating the phase separation process. The total system charge was neutralized adding Na^+ and Cl^- ions at a concentration of 150 mM. The system was energy-minimized by the steepest descent method for 1500 steps and then equilibrated on NPT ensemble for 0.5 ns using V-rescale thermostat[51] and Berendsen[52] semiisotropic barostat as coupling methods. Each type of lipid is coupled separately in temperature as recently suggested in phase separation studies[53]. Each molecular system was subjected on 2 μs of MD production in the NPT ensemble: the temperature was kept at 293 K using velocity rescaling thermostat (τ_T = 1.0 ps) and the pressure at 1 bar using Parrinello-Raham barostat (τ_P = 12 ps)[54]. The electrostatic interactions were evaluated by particle mesh Ewald (PME) method using 1.2 nm as cut-off[55].The van der Waals interactions were calculated by applying a cut-off distance of 1.2 nm and switching the potential from 1.0 nm. MARTINI force-field topology was used to parametrize the molecular systems[56], choosing the polarizable water model. The TRO mapping was reported in the supplementary material (**Figure SI10c**). All MD simulations were carried out using GROMACS 2020 software package[57].

Molecular dynamics simulations – lipid monolayer

In order to verified whether TRO is able to interact with a lipid monolayer, two TRO molecules were inserted in the water slab environment in vacuum with two symmetric monolayers at the two water−vacuum interfaces (**Figure SI11a**). The molecular system was built starting from a lipid bilayer, using a bilayer builder[53]. The monolayers consisted of dibehenoyl-phosphatidylcholine (DBPC) and dilinoleyl-phosphatidylcholine (DIPC) with a mole ratio of 3:1. The total system charge was neutralized adding Na^+ and Cl^- ions at a concentration of 150 mM in the water slab. The system was energy-minimized by the steepest descent method for 1500 steps and then equilibrated at 293K and 1 bar on NPT ensemble for 0.5 ns using V-rescale thermostat[51] and Berendsen[52] semiisotropic barostat as coupling methods. Finally, the molecular system was investigated by 3 μs of MD production in the NVT ensemble at 293 K.

Results and Discussion

Langmuir monolayers of membrane lipids

Monolayers of the binary, ternary and quaternary mixtures were preliminary studied on phosphate buffer and water subphases. For all investigated systems, the analysis of surface pressure – area isotherms for the different monolayers provided information on phase transitions, lateral diffusion and mixing interactions that lead to changes in the order of hydrocarbon chains and lateral compressibility[58]. Isotherms were analyzed as described in the *Materials and methods* section.

Since the behavior of the whole model is determined mostly by the two major components of the lipid mixture, we preliminarily studied the DOPC/SM binary system at water-air interface (F**igure SI2**) and at the buffer phosphate-air interface (F**igure SI3**). As expected, the pure DOPC isotherm presents a very expanded phase in the entire surface pressure range on both subphases while the pure SM monolayer presents a transition from liquid-expanded (LE) to liquid-condensed (LC) phase around 16 mN/m, disclosed also by the large surface compressional modulus (C_s^{-1}) values. Surface pressure–area isotherms for the binary DOPC/SM monolayers at the air-water interface (F**igure SI2**) are consistent with those previously reported[3,5,59,60,61,62] . Thermodynamic analysis of surface pressure-area isotherms for the binary DOPC/SM mixtures on phosphate buffer is reported in **Figure SI3** and revealed that at larger SM molar fractions, the experimental surface area values, $A_{mix,}$ at constant surface pressure show slightly positive deviations from ideality in the entire surface pressure range suggesting miscibility. The behavior of Cs^{-1} and of the excess of Gibbs free energy ΔG^{E}_{Mix} confirm that the bidimensional miscibility of the two lipids although with minor repulsive interactions.

To investigate the interfacial behavior of the monolayer we combined the Langmuir experiments with Brewster Angle Microscopy (BAM) obtaining a morphological characterization of the monolayer. BAM experiments exploit the differences in p-polarized light reflected by the liquid-air interface to reconstruct the image of the monolayer with high lateral resolution. BAM images can be related to characteristic phases in the Langmuir isotherm, in which bright areas in the image identify more ordered and condensed domains, whereas dark areas reveal expanded phases. BAM images reported in **Table SI1** confirmed the presence of homogeneous expanded phases in the entire surface pressure range for DOPC, whereas for SM bright condensed domains increase in number as surface pressure increases. In the case of the mixtures the number of condensed domains depend on the SM molar fraction although they maintain the same average size. The molar ratios of DOPC and SM in the lipid mixtures of interest are DOPC/SM 2:1 for the L_d+S_o phase and 90:8 for the homogeneous L_d phase, for the latter composition we observed only homogeneous liquid expanded phases in BAM images in the entire surface pressure range whereas condensed ordered domains appeared in the DOPC/SM 2:1 system above π = 20 mN/m.

Monolayers of the ternary and quaternary lipid mixtures on phosphate buffer were investigated to confirm the effect of cholesterol and GM1 on the monolayer organization in the absence of Trodusquemine. The DOPC/SM ratio was kept constant to 2:1 for all systems, as reported above at this DOPC/SM molar ratio repulsive interactions are expected at surface pressure larger than 20 mN/m. Although the role of cholesterol in the regulation of fluidity in cell membranes and formation of microdomains is well known and studied[63,64], the comparison between binary and ternary mixtures will confirm the effect of cholesterol for this specific monolayer composition. Cholesterol is known to interact differently with the various membrane lipids, associating particularly strongly with saturated, high-melting phospho- and sphingolipids and weakly with highly unsaturated lipid species[65,66,67,68]. Systems composed of cholesterol and lipids naturally present in the native external membrane leaflet have been investigated by many authors using vesicles[69,70], Langmuir monolayers[71,72] and supported lipid membranes[73,74]. Typical Langmuir monolayer isotherms and surface compressional moduli for the binary, ternary and quaternary lipid mixtures with DOPC:SM 2:1 are reported in **Figure SI4** and **TableSI2**. The results confirmed that when 1% of Chol is added to the DOPC/SM 2:1 mixture, the isotherms are shifted towards smaller areas confirming that Chol closely packs with the membrane lipids. The polar hydroxyl of cholesterol bestows on the sterol amphipathic character, which enables it to orient in bilayer membranes parallel to the phospholipids[57]. Cholesterol was confirmed to increase the Cs^{-1} of the monolayer, a key factor in determining raft stability and organization, due to the association of Chol with SM in ordered and randomly distributed rafts domains.

Comparison between the ternary, (DOPC/SM/Chol 66:33:1) and quaternary (DOPC/SM/Chol/GM1 65:33:1:1) mixtures highlighted the effect of GM1 on the physical properties and structure of the monolayer. Gangliosides are an important class of lipids found in the outer leaflet of the plasma membrane believed to colocalize preferentially with cholesterol and sphingomyelin in ordered membrane domains, but a detailed understanding of the lateral organization of GM-containing membranes is still ambiguous[1628]. Molecular dynamic simulations of GMs in model membranes composed of coexisting liquid-ordered and liquid-disordered domains demonstrated that GMs have a preference to partition into the ordered domains[28]. We found that the addition of even small quantities of GM1 (1%) to the ternary DOPC/SM/Chol system led to a minor displacement towards larger areas of the isotherm especially for surface pressure larger than 15 mN/m confirming that GM1 interacts preferentially with ordered domains (**Figure SI4**). Interestingly, the fluidity of the quaternary system is slightly larger than the ternary mixture (see **Table SI2**) suggesting that the small raft domains are less tightly packed in the quaternary mixture, a behavior previously predicted also by MD simulations[75].

Langmuir monolayers of Trodusquemine. TRO, a molecule formed by a polyamine tail and a sulphate group linked together by a sterol core[9] can be considered as an asymmetrical bola-amphiphile bearing a negatively charged group on one side of the sterol rigid core and a positively charged polyamine on the other side (**Figure 1a**). Bolaamphiphiles are known to significantly stabilize lipid membranes[76]and to form peculiar self-assembled structures, such as liquid crystalline phases in the bulk state[77] and gels[78]. More recently, they have also been reported to form "bolasomes", either alone or together with fusogenic lipids such as DOPE[79].

To investigate the interfacial behavior of Trodusquemine, we explored the formation of spreading monolayers of TRO, in the absence of lipids, at the buffer-water interface. Rarely, soluble amphiphilic molecules may form insoluble Langmuir monolayers at the interface[8081] without partitioning in the subphase. Insight in such behavior would be particularly relevant in connection with the issue of TRO interaction with cellular membrane and might provide a rationale, on a molecular basis, for the driving force for the insertion or penetration of TRO in a phospholipid bilayer[9, 13]. Spreading of TRO from a chloroform/methanol dispersion at the phosphate buffer-air interface resulted in a stable Langmuir monolayer as shown in **Figure 1a**. Surface pressure increases monotonically as available surface area decreases showing a plateau region at $\pi = 8$ mN/m that is indicative of a 2D phase transition.

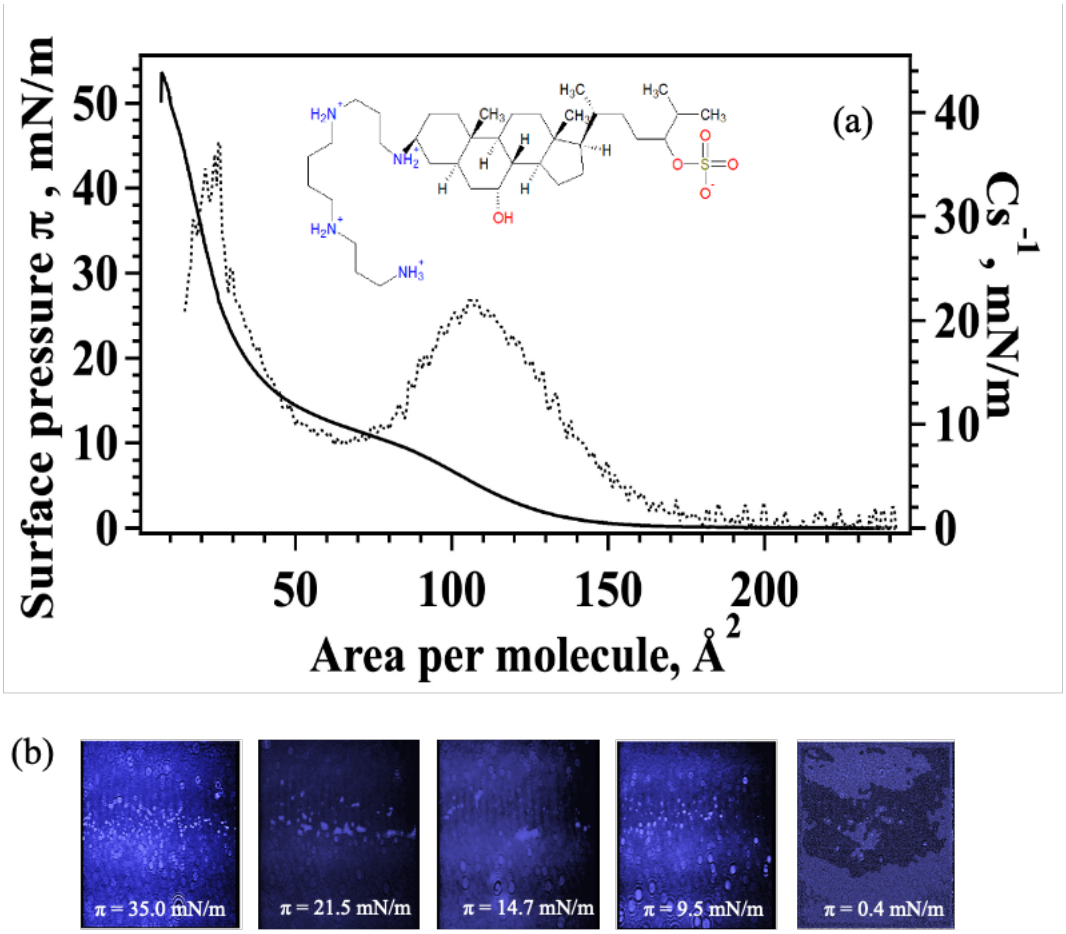

Figure 1. (a) Surface pressure – surface area (solid black line) and surface compressional modulus – surface area (dotted black line) isotherms for TRO on buffer phosphate. Inset: chemical formula of TRO. At pH 7, 97% of TRO molecules bear four positive charges besides the negative charged group and has, therefore, a net charge of +3. (b) BAM images (513 µm x 435 µm) of TRO at different surface pressure. All measurements were run at pH 7 and T= 20 °C.

The presence of a phase transition is supported also by the maximum of the surface compressional modulus (Cs^{-1} = 22 mN/m) that levels off along the plateau reaching a slightly higher second maximum at π= 25 mN/m (**Figure 1a**, right y-axis). Although the presence of two maxima would suggest the presence of two phase transitions, the low values of the Cs^{-1} indicate that TRO forms a fluid and elastic monolayer in the entire surface pressure range[82].

Compression-expansion cycles were performed on TRO monolayers arresting compression below the collapse surface pressure. The results (**Figure SI5**) showed small hysteresis and total recovery of the

monolayer in the second compression allowing to exclude loss of material in the subphase upon compression and suggest a reversibility of both phase transitions.

The area occupied by the TRO molecule at the interface before the plateau, obtained by extrapolating the linear portion of the isotherm to zero surface pressure, is 134 $Å^2$/molecule. This value reveals that TRO molecules lie isolated at the interface with the hydrophobic core almost parallel to the interface. Upon compression, the molecules get closer and further approach of the polar headgroups becomes energetically unfavorable due to their mutual repulsion. Further compression induces a first order phase-transition indicating either a tilting of the molecule at the interface or the formation of surface aggregates or of multilayers. It is tempting to assign such transition to bilayer formation as suggested by the difference in surface areas per molecule (A_1 and A_2) at both ends of the plateau (A_1 ca. $2A_2$ at π = 10 mN/m), after the plateau the limiting area before collapse plummets to 42 $Å^2$/molecule, a value that may indicate either the transition to a different arrangement of the TRO molecules or dissolution of 3D aggregates into the subphase.

Previous studies also report that bolaamphiphiles form Langmuir monolayers with different molecular packing and conformations: bolaamphiphiles with rigid central cores are reported to adopt flat-lying molecular conformations on water surfaces evolving to side-by-side molecular assemblies upon compression sacrificing contact of the headgroups with the aqueous subphase[83]. More rarely, compression is reported to result in a reverse U-shaped folded state[84], a deformation more commonly observed for flexible hydrophobic spacers, or to the collapse of monolayer structures in multiple layers and higher aggregates[85].

Representative BAM images of TRO monolayers on phosphate buffer subphase are reported in the insets of **Figure 1b** both below and above the plateau region. In the low surface pressure regime, the images reveal the presence of a dark field of gaseous phases and bright blurred stripes of liquid expanded TRO domains, a feature also previously observed for single chain bola-amphiphile[86]. As pressure increases, bright spots start to form although the domains are too small to detect any anisotropy even if present, the condensed domains localize at the edge of the liquid-expanded phase and increase in number as compression proceeds. Along the plateau region the bright spots condense to form larger TRO aggregates that disappear above 25 mN/m corresponding to the phase transition evidenced by the second maximum in the Cs^{-1} plot.

Assuming that TRO conformation in the liquid-expanded phase is associated with the extended form, BAM images suggest a transformation from a 2D liquid expanded phase to condensed domains with a different morphology. For conventional symmetrical bolamphiles reversible extended-to-bent transitions are generally observed[77][87] but the central hydrophobic core of TRO is too rigid to allow for a U-shape transition and bending can only involve the polyamino polar group at one extremity of the molecule. A reversed U-

shape conformation was observed for bola-amphiphiles with rigid biphenyl cores arranged parallel to the water surface but in that case flexible siloxane units decouple the rigid core from the head groups[78].

Interestingly, upon further compression of the monolayer the larger aggregates disappear from the surface leaving only a high density of circular domains. Such behavior might be caused by dissolution in the bulk phase of the heavier aggregates but the presence of a second maximum in the Cs^{-1} points to a reversal of the aggregate structuring via a first-order phase transition. This unusual behavior has been seldom reported in the literature: recent studies[88] on asymmetrical bola-amphiphile observed the co-existence of multiple phases in the monolayer before the amorphous collapse of the monolayer. The authors detected a regular secondary bola-conformation atop the extended organization, the multilayer evolved in the forms of nodules decorating the edges of the extended phase as we also observed in the BAM images reported in **Figure 1b**

Further information on the evolution of the surface structures was obtained from the statistical analysis of the BAM images. **Figure 2a** reports the percentage fraction and the average circularity of the brighter domains as function of the surface pressure. A deeper inspection of the condensed domain highlights the presence of aggregates differing both in thickness and size (**Figure 2b**). A typical example of data elaboration both for the mean domain size and thickness of the Trodusquemine aggregates is reported in the supplementary material (**Figure SI6**). The thickness of each monolayer domain was estimated as reported in the experimental part.

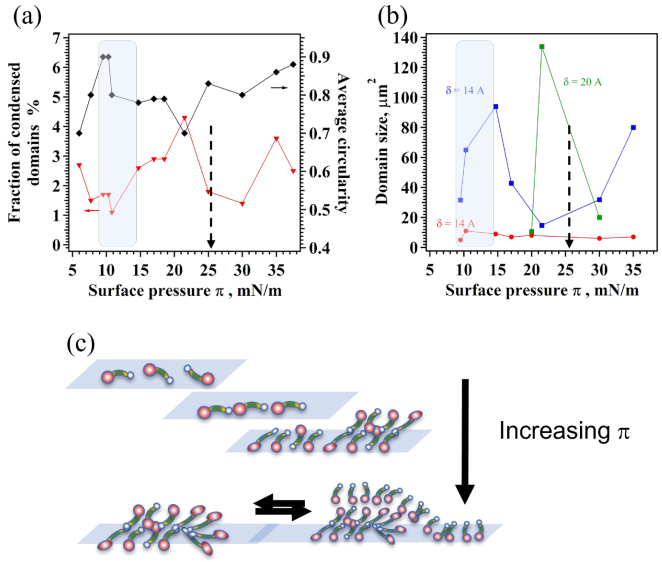

Figure 2. (a) Average area fraction and circularity for the condensed domains (b) Average size for condensed domains and corresponding thickness δ. The shaded area represents the monolayer to bilayer phase transition (plateau region in the π-A isotherm), dashed arrows indicate the second phase transition at π =25 mN/m. (c) Cartoon representing the compression steps and the reversible bilayer-trilayer transition.

At low surface pressure (π <5 mN/m), the condensed domains, localized at the edge of the expanded stripes, increase in area fraction evolving in larger structures with lower circularity along the plateau (shaded area **Figure 2a-b**). Further compression leads to a decrease of the size of the larger domains flanked by an increase in circularity while the overall fractions of condensed domains is constant. Combined analysis of the mean domain size and the thickness of the aggregates (**Figure 2b**) revealed that an uniform expanded monolayer is present in the entire surface pressure range, but the plateau marks the onset of domains with bilayer thickness that increases in size along the plateau. As π further increases, a fraction of the bilayer patches decreases in size while a third population, with trilayer thickness, rapidly grows (134 μm^2), when π approaches the second phase transition (π=25 mN/m) the trilayer reverts to bilayer domains before the final collapse of the monolayer.

Taken together the results trace a path for the evolution of TRO at the interface as a function of surface pressure as depicted in **Figure 2c**. In the expanded phase below the plateau, TRO assumes an extended conformation at the interface as proposed for the adsorption monolayer, with the polyamino chains probably dangling in the water subphase with an average thickness of 7 Å. At the domain boundaries, TRO has sufficient space and conformational freedom to bend over and a transition to larger structure of higher thickness is initiated.

The bilayer with average thickness 14 Å, eventually evolves in a tri-layer either with a head-to-head conformation, as shown in the scheme, or with a head-to-tail arrangement, both arrangements have been reported for lamellar or crystal structure of bolamphiphiles[71]. The trilayer (average thickness = 20 Å) exists in a small interval of surface pressure and reverts with a first order phase transition to bilayer patches in an expanded monolayer background. This transition is reversible as also shown by the complete recovery of the monolayer after the first compression-expansion cycle (**Figure SI5**). Reversible trilayer formation was previously observed for T-shaped facial amphiphiles and bola-amphiphiles with rodlike aromatics arranged parallel to the surface[78]. The authors suggested that trilayer formation resulted from a lifting and/or rollover process and explained the reversibility of the π-A isotherm by line tension of the trilayer domains coexisting with the residual expanded monolayer. Further compression results in the reorganization of the hydrophobic cores into a more vertical orientation and lead to the packing of the condensed domain and collapse to a 3D bulk phase.

Trodusquemine in L_d+S_o lipid monolayers. Mixed monolayers of DOPC/SM/Chol/GM1 65:33:1:1 and Trodusquemine were studied on phosphate buffer subphases at increasing concentrations of TRO in the lipid layer. Surface pressure area isotherms are reported in **Figure 3** together with behavior of C_s^{-1} as a function of surface pressure. Langmuir isotherms of the DOPC/SM/Chol/GM1 65:33:1:1 system change in shape and position as TRO concentration in the monolayer increases (**Figure 3a**). A phase transition at low surface pressure is detected in all isotherms becoming a plateau for TRO molar fraction = 0.67 suggesting that, at this TRO concentration, a fraction of TRO segregates in the monolayer forming bilayer domains as observed also in other systems[40]. Monolayer elasticity and fluidity also increase for TRO molar fractions greater than 0.5, reaching values similar to those of the single TRO monolayer (**See Figure 2b**); on the contrary the film elasticity at high lipid content is always higher than that found for the lipid mixture alone (**Figure 3b**), indicating that TRO is miscible in the lipid monolayer and even a small concentration of TRO alters the monolayer properties.

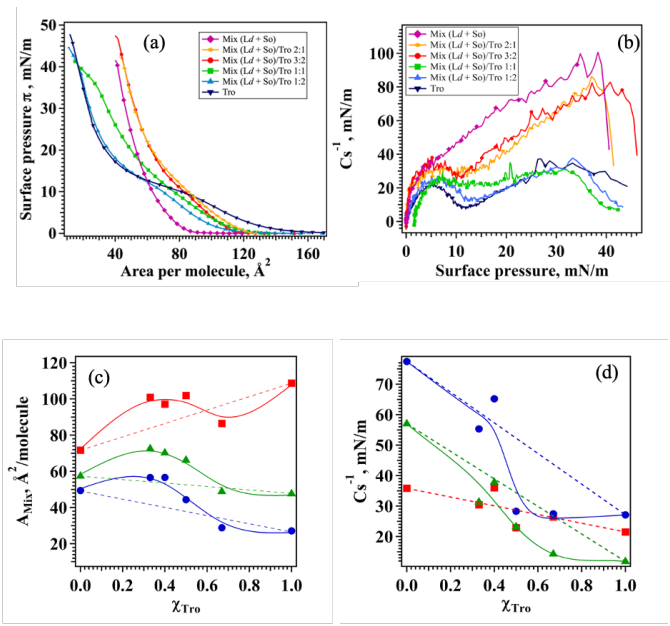

Figure 3. (a) Surface pressure – area isotherms for quaternary mixtures of lipids containing L_d and S_o phases cospread with increasing concentration of TRO at the air-phosphate buffer interface. (b) Surface compressional modulus – surface pressure isotherms for quaternary mixtures of lipids containing L_d and S_o phases co-spread with increasing concentration of TRO at the air-phosphate buffer interface. Measurements were run at pH 7 and T= 20 °C. (c) Excess molecular area, A_{Mix}, and (d) surface compressional moduli, Cs^{-1}, as a function of TRO molar fraction at 5 mN/m (red squares), 15 mN/m (green triangles) and 25 mN/m (blue circles).

The behavior of the experimental surface areas, A_{Mix}, at constant surface pressure and the change in Cs^{-1}as a function of TRO molar fraction is reported in **Figure 3**. Deviations of A_{Mix} from additivity (**Figure 3c**) were mainly positive at each surface pressure for TRO molar fraction below 0.5. This implies that the components were miscible but repulsive interaction energies prevailed in the monolayer between the lipid components and TRO. Such behavior indicates that TRO interacts with the lipid components both in the LE and LC phases for these molar fractions. For $\chi_{TRO} < 0.5$ all the reported data confirm the bidimensional miscibility of the components that establish repulsive interaction as shown also by the ΔG^{E}_{Mix} values reported in **Figure SI7.** More importantly, we found a local maximum for the areas when Lipid:TRO molar ratio equals to 3:2 ($\chi_{TRO} = 0.4$), disclosing that incorporation of TRO in the lipid monolayer reaches a maximum at this molar ratio. For TRO molar fraction larger than 0.5, A_{Mix} values follow ideal mixing suggesting either immiscibility or ideal miscibility, however the plots in **Figure 3d** show that for $\chi_{TRO} > 0.5$ the C_s^{-1}values overlap with the value obtained for pure TRO monolayers partial demixing of TRO from the lipid monolayer can be postulated. Also, according to Crisp phase rule, mutual incompatibility between the components for χ_{TRO} larger than 0.5 was deduced from the invariance of $\pi_{coll.}$ (**Figure SI7**) and the values of the limiting areas A_0 at higher TRO content reported in the same figure.

BAM images of monolayers of quaternary lipid system in the absence of TRO (**Figure SI8**) show that condensed domains (S_o) surrounded by a liquid disordered phase (L_d) are already present at 5 mN/m and their density and size increases with increasing surface pressure, as expected, reaching the largest density in the 20-30 mN/m surface pressure range, a value that mimics the cellular membrane. Closer inspection of BAM images at 15 mN/m and 25 mN/m for the lipid:TRO mixture reveals clearly that the presence of TRO in the monolayer perturbs the shape and size of the S_o domains

(a)

Monolayer composition	Surface pressure	
	15 mN/m	25 mN/m
Mix (L*d* + So)	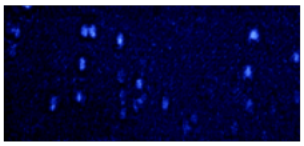	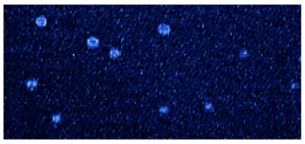
Mix (L*d* + So)/TRO 3:2	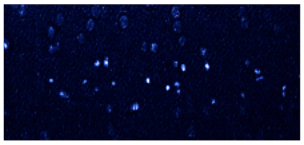	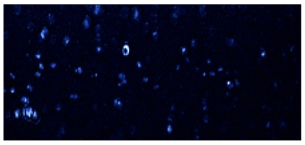

(b)

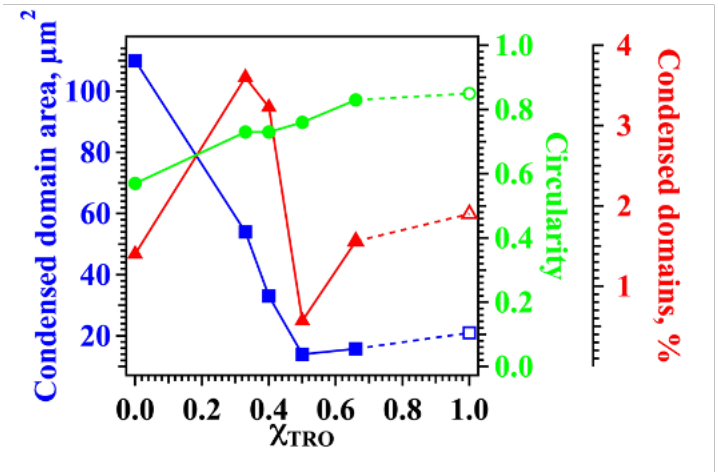

(c)

Monolayer composition	Mismatch, Å
Mix (L*d* + So)	5 ± 2
Mix (L*d* + So)/TRO 2:1	7 ± 2
Mix (L*d* + So)/TRO 3:2	12 ± 3
Mix (L*d* + So)/TRO 1:1	5 ± 2
Mix (L*d* + So)/TRO 1:2	5 ± 2

Figure 4. (a) Typical BAM images obtained at 15 mN/m and 25 Mn/m for the mixture lipid/TRO mixture 3:2. (b) Average condensed domain area (blue squares), total fraction (red triangles) and average circularity (green circles) of the condensed S_0domains as function of the TRO molar fraction. (c) Mismatch between the thickness of the condensed domains and the expanded L_d phase as a function of TRO in the lipid monolayer.

BAM images were analyzed as already described for TRO monolayers, (see lower panel of **Figure SI8** for a typical example of the statistical analysis combined with the thickness determination). The results collected in **Figure 4a** show the average area of the condensed S_o domains (blue) together with the total content of S_o domains (red) and the circularity of the lipid raft (green). The analysis reveals that the

dimension of the larger S_o domains decreases with increasing TRO concentration, reaching a minimum for TRO molar fractions of 0.5, and then increasing only slightly reaching the size of pure TRO bilayer patches at χ_{TRO} = 1. More importantly, the total fraction of S_o domains is maximum for χ_{TRO} close to 0.4, namely Mix (L*d*+So)/TRO 3:2, corresponding to maximum uptake of TRO found from the analysis of the spreading isotherms. The average circularity of the domains increases with the content of TRO in the lipid monolayer leveling-off after χ_{TRO} = 0.5. These results agree with those previously obtained with AFM where small concentrations of TRO were found to have all these same effects on S_o domains[15].

We also estimated the mismatch, defined as the difference in thickness between the S_o domains and the L_d phase in the monolayer, as a function of TRO concentration (**Figure 4b**). In the case of lipid monolayers, we found a mismatch that agrees with literature data for similar systems[89] and with AFM results obtained for Supported Lipid Bilayers of the same composition[13]. Interestingly, the mismatch in thickness of the S_o domains increases as TRO is incorporated in the monolayer, reaching a maximum for χ_{TRO} of 0.4, after which the mismatch is again similar to pure lipid monolayers devoid of TRO.

Overall, these results suggest that TRO distributes both in the disordered L_d phase and in the S_o phase for χ_{TRO} lower than 0.5, for larger molar fractions TRO separates from the L_d phase forming bilayer (or trilayer) aggregates probably coexisting with the TRO loaded S_o domains. When incorporated in the condensed S_o domains TRO induces a decrease in their size, in their density and an increase in their thickness. The mismatch at maximum TRO uptake is ca. 12 Å, suggesting a lipid reorganization along the normal to the interface upon TRO penetration. This behavior suggests a preferential adsorption of TRO at the raft borders affecting the line tension of the condensed S_o domains. Adsorption of TRO along the line tension of lipid rafts is not unexpected due to the overall favorable decrease of surface energy upon TRO localization at the sites of higher energies, this promotes fragmentation of the rafts in smaller domains stabilized by TRO as observed also in other interfacial systems[90,91,92].

Previous studies[13] on TRO interactions in phospholipid bilayers of the same composition showed that TRO penetrates the bilayer only partially, exposing part of the polyamine chain towards the water-phase. A similar conformation may be assumed also for TRO at the border of the S_o domains: the TRO hydrophobic sterol segment interacts with the exposed alkyl chain of the S_o domain protruding from the L_d phase, leaving the polar groups at the interface or dangling in the water phase.

Trodusquemine in homogeneously distributed in L_d monolayers. To confirm that the presence of S_o domains significantly influences the interaction of the lipid monolayer with TRO, the biomimetic model

containing only the L_d phase (DOPC/SM/Chol/GM1 90:8:1:1) cospread with TRO was investigated focusing on the molar fraction that exhibits the largest TRO interactions, i.e $\chi_{TRO} = 0.4$. The results reported in **Figure SI9** confirm that TRO is dispersed in the L_d monolayer, and that mixing is almost ideal in the entire surface pressure range (see **Table SI3**), suggesting either immiscibility or ideal miscibility. C_s^{-1} values are lower than in the case of DOPC/SM/Chol/GM1 65:33:1:1(L_d+S_o) mixtures and even lower in presence of TRO. The excess molecular areas for the investigated concentration of TRO in the DOPC/SM/Chol/GM1 90:8:1:1 (L_d) mixture behave almost ideally in the entire surface pressure range suggesting immiscibility between the components (**Table SI3**) as observed also for DOPC/SM/Chol/GM1 65:33:1:1 mixture for $\chi_{TRO} > 0.5$ (**Figure 3**). These data indicate that Trodusquemine distributes easily in the L_d phase richer in DOPC but no preferential interactions between DOPC rich phases and TRO are established, probably due to flat orientation of TRO in these expanded phases that does not allow for effective hydrophobic interactions with the lipid molecules.

BAM images for this lipid system shows the presence of a single homogenous L_d phase, at low surface pressure; at surface pressure closer to the lateral pressure in cell membranes, the L_d monolayer is only slightly perturbed by the presence of TRO aggregates (**Figure SI9**).

The presence of GM1 in the lipid mixture affects interactions between TRO and S_0 domains.

We studied monolayers of the ternary DOPC/SM/Chol mixture, focusing both on the L_d DOPC/SM/Chol 91:8:1) and the L_d+S_o (DOPC/SM/Chol 66:33:1) compositions, both alone and in the presence of TRO at χ_{TRO} of 0.4 to ascertain if the lack of GM1 affects the interactions of TRO with the S_o domains.

The biological role of GM1 in neurodegenerations has been since long established[35]: ganglioside accumulation was observed in lipid rafts isolated from the frontal and temporal cerebral cortex of AD individuals[93] while lipid raft-associated ganglioside GM1 has been suggested to facilitate beta-amyloid aggregation and oligomer cytotoxicity via bilayer destabilization by soluble oligomers within GM1-rich ordered raft regions[94].

Molecular dynamic simulations of GMs propose that GMs partition into the S_o domains with the GM headgroup affecting the phase separation while the tails determine the preferential localization[28]. Moreover, AFM experiments proved that GMs aggregate into gel-phase S_o domains in PC monolayers, even when the concentration is as low as 1%[28].

An expected contraction of the isotherm towards smaller areas was observed in the case of the ternary L_d+S_o mixture compared to the ternary $L_{d\,phase}$ in the absence of TRO (**Figure 5**). The addition of TRO shifts

the isotherm to larger areas for the ternary L_d+S_o mixture, whereas an area contraction occurs only at π>10mN/m in the case of the ternary Mix containing only the L*d* phase, similarly to the observation for the corresponding quaternary Lipid mixture.

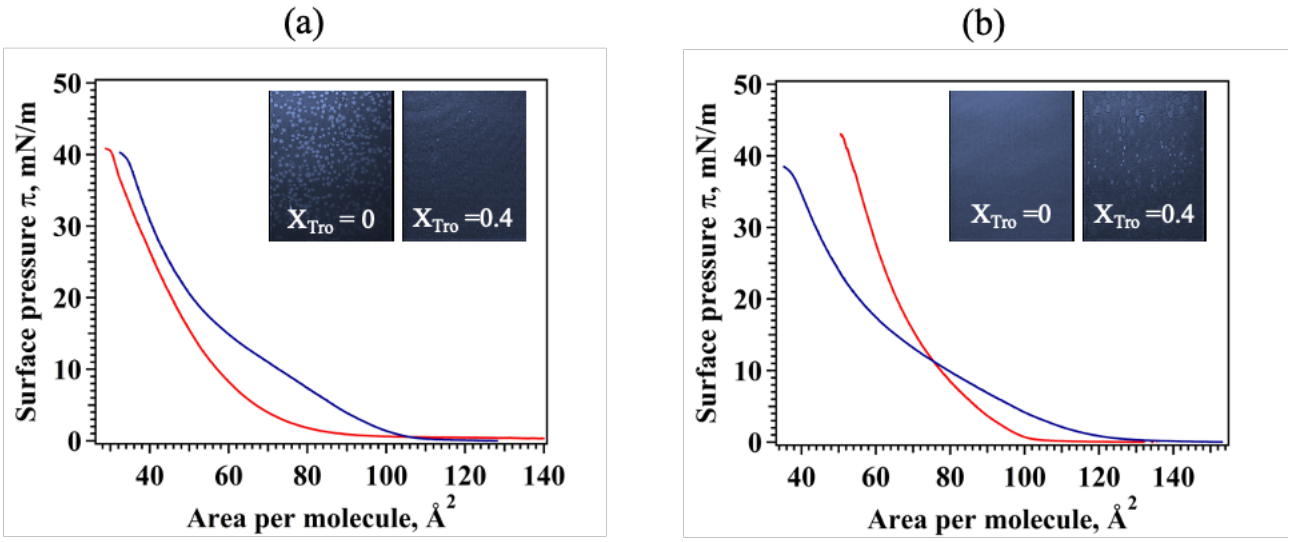

Figure 5. (a) Surface pressure – surface area isotherms of the ternary DOPC/SM/Chol 66:33:1 mixtures containing both the L_d and S_o phases with TRO (blue lines) and without TRO (red lines) at the air-phosphate buffer interface. (b) Analogous plot for a ternary DOPC/SM/Chol 91:8:1 mixture featuring only the L*d* phase. χ_{TRO} = 0.4 in all experiments. BAM images collected at π = 25 mN/m, size 535 µm x 430 µm.

Closer inspection of the behavior of the surface compressional modulus in **Table SI2** and in **Figure 3b** shows that GM1 and TRO exert a similar effect on monolayer fluidity of the DOPC/SM/Chol monolayer containing both the L_d and S_o with Cs^{-1}= 103 mN/m and Cs^{-1} = 80 mN/m at π=25 mN/m. Furthermore, in the absence of GM1, BAM images clearly show that TRO dramatically reduces the size of the So domains, as well as the total condensed fraction. On the other hand, when TRO is mixed with the ternary L_d phase at π > 10 mN/m we assist only to the formation of larger domains (ca. 20-25 μm^2) with thickness comparable to TRO bilayer aggregates (see **Table SI4**) as already observed also for the quaternary mix L*d*.

The results indicate that both TRO and GM1 concur in decreasing the size of the raft domains, a hypothesis further supported by other authors that found that GM1, similarly to TRO, brings morphological changes in the condensed film but not in the liquid expanded film[95].

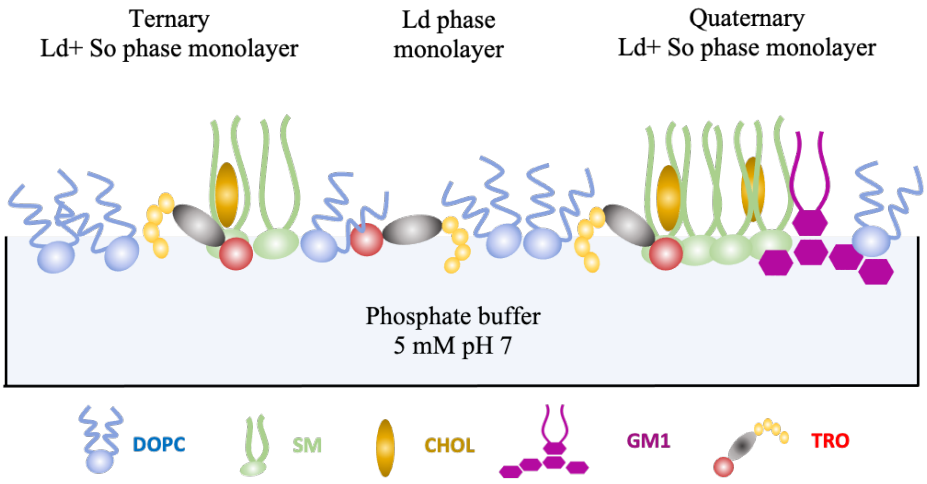

Figure 6. Schematic representation of the reorganization of the outer layer of the plasma membrane model induced by Trodusquemine in L_d and L_d+S_o phases.

Apparently, TRO induces an even greater reduction of the size of the S_0 domains, suggesting that the presence of GM1 hinders the localization of TRO at the S_0 domain boundaries, probably due to electrostatic repulsion between the sulphate group and the negatively charged head groups of GM1. In fact, previous work[96] showed that anionic GM1 in the membrane promotes the association of positively charged amphipathic neurotransmitters like histamine, acetylcholine, and dopamine.

Previous works from this group[15] showed that when Large Unilamellar Vesicles with the same DOPC/SM/Chol/GM1 composition are formed in the presence of TRO, a process analogous to the cospreading reported in the present work, TRO interacts preferentially with the (L_d+So) phase modifying the distribution of the lipids. In addition, FRET experiments revealed that, in the presence of TRO, Chol molecules get closer, due to the decrease in the size of the raft, while Chol-GM1 distance increases due to the lipid redistribution in the raft.

Taken together the results show that TRO penetrates the monolayer localizing at the lipid raft borders establishing hydrophobic interactions between the sterol group and the exposed alkyl chains of the lipid matrix but keeping the sulphate moiety distant from the GM1 polar group as depicted in the sketch of **Figure 6**.

Such findings are biologically relevant since lipid rafts are recognized as preferential platforms that recruit toxic oligomers resulting in cell damage[97]. Recent results by Pham et al. also demonstrated the tight binding of beta-amyloid oligomers to the GM1-clusters at the Lod domain are early molecular events of the

beta-amyloid aggregation process on neuronal membrane surfaces that trigger the onset of Alzheimer's[98]. Furthermore, Evangelisti et al. observed how even a modest depletion of GM1 content and interference with GM1 exposure or negative charge, precluded the interaction of amyloid aggregates with the plasma membrane and the resulting cell damage[93].

Therefore, our results offer a rationale for the therapeutic action of Trodusquemine in neurodegenerations, involving the modification of the interface between L_o and L_d phases and the redistribution of lipid raft components resulting in the inhibition of the sequential pathological events of AD, a mechanism recently proposed also by other authors[99]

Molecular dynamic simulations of Trodusquemine interaction with lipid rafts

Figure SI10b shows the lateral and the top view of the initial system configuration, and the two types of phospholipids are randomly distributed on the membrane plane. During the MD production, the lipids are able to reorganize themself and their spatial distribution. After 700 ns of MD simulation, the area per lipid converges to 52.25 ± 0.17 Å^2. The final lipids distribution shows a net phase separation where each type of phospholipid is clustered in Liquid Order (L_o) or Liquid Disorder (L_d) phase (**Figure SI10c**).

The separated phase system was used to understand whether TRO molecules can still interact with the lipid membrane. The phase separation results in a marked difference in thickness between lipids in the L_o state and lipids in the L_d state (**Figure 7c**). The thickness gap between the two lipid types causes a hydrophobic portion of L_o lipids exposed to solvent. Despite the phase separation of the cell membrane, the ability of TRO to partially penetrate the membrane is preserved. MD simulations shows the TRO preference to interact with the boundary between the two phases (**Figure 7a**). In particular, TRO is able to interact with the hydrophobic surface exposed to solvent of L_o state along the phase separation boundary (**Figure 7a-b**). Furthermore, TRO interactions increase the thickness mismatch between L_o and L_d domains, as also observed by experimental evidence (**Figure 4b**), up to 1.67 nm with 4 TRO molecules (**Figure 7c**).

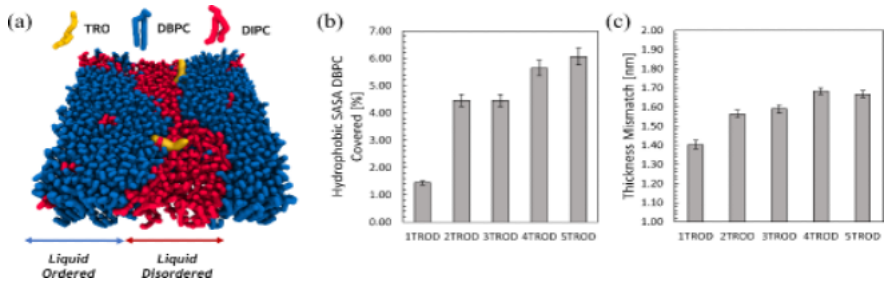

Figure 7. (a) Final configuration of TRO localized at the phase separation boundary (b) Percentage of hydrophobic SASA of L_o covered by the TRO interaction as a function of the number of TRO considered (c) Thickness mismatch between L_o and L_d domains**.**

Furthermore, the ability of TRO to interact with a lipid monolayer was tested, inserting two TRO molecules in a water slab environment between the two monolayers. **Figure SI11a** shows the starting configuration of the MD simulation. During 3 μs of MD simulation, the ability of TRO to interact with the phase separation edge agrees with the molecular events observed in presence of a phospholipid bilayer (**Figure S11b**). In this context, the lipid bilayer is also well representative of TRO behavior in the presence of phase separation of a lipid monolayer.

CONCLUSIONS

We have first shown that TRO, an asymmetrical bolamphile, spreads at the phosphate buffer-air interface in the absence of lipids, forming an expanded fluid monolayer that converts reversibly in bilayer and trilayer structures.

Co-spreading TRO with lipid mixtures of DOPC/SM/Chol/GM1 with compositions promoting both the L_d or L_d+ S_o phases resulted in stable Langmuir monolayers inducing a series of physico-chemical changes that include molecular packing and lipid distribution. We found that TRO is homogeneously dispersed in the L_d phase of the monolayers without preferential interactions with the lipid molecules. On the contrary, in the presence of a coexistence of L_d and S_o phases, TRO forms miscible monolayers with repulsive interactions with the lipid components for TRO molar fraction lower than 0.5. The maximum interaction of TRO with the lipids is observed for lipid: TRO molar ratio of 3:2. TRO induces a reorganization of the S_o domains, reducing their size, increasing their density, their circular shape and augmenting the thickness mismatch with the L_d phase. This effect was observed also in MD simulation of similar L_d+ S_o phases that found a thickness mismatch very close to the experimental one. Both approaches converge in describing TRO as localized along the border of the S_o domains. Such behavior is ascribed to preferential adsorption of TRO along the line tension of the S_o domain borders, thanks to preferential interactions of the sterol moiety of TRO with the exposed hydrophobic portion of the lipids.

Removal of GM1 from the mixed TRO/lipid L_d+S_o monolayer resulted in an even greater TRO-mediated reduction of the size of the S_o domains, suggesting that the presence of GM1 hinders the localization of TRO at the lipid rafts boundaries.

Overall, the results presented in this work show that the interactions of TRO with the lipid monolayer model of the outer membrane induces a lipid composition-dependent and long-range reorganization of the lipid monolayer that should be considered in the context of the protection offered by TRO against binding of aberrant misfolded proteins as well as in the case of many signal transduction pathways in cells that involve lipid rafts.

Acknowledgements

This research was funded by the Regione Toscana (FAS-Salute 2014, project SUPREMAL); the University of Florence (Fondi di Ateneo). We thank MIUR-Italy "Progetto Dipartimenti di Eccellenza 2018-2022" allocated to Department of Chemistry "Ugo Schiff" (Florence), and to the Department of Experimental and Clinical Biomedical Sciences "Mario Serio" (Florence). The computer simulations were supported by a grant from the Swiss National Supercomputing Centre (CSCS).

Conflict of Interest.

The authors declare no conflict of interest

References

[1] J. Brettschneider, K. Del Tredici, V.M.-Y. Lee, J.Q. Trojanowski, Spreading of pathology in neurodegenerative diseases: a focus on human studies, Nat Rev Neurosci. 16(2) (2015) 109-120

[2] C. Soto, Unfolding the role of protein misfolding in neurodegenerative diseases, Nat. Rev. Neurosci. 4 (2003) 49-60

[3] Coskuner O, Uversky VN. Prog Mol Biol Transl Sci., Intrinsically disordered proteins in various hypotheses on the pathogenesis of Alzheimer's and Parkinson's diseases, 166 (2019) 145-223

[4] F. Chiti, C.M. Dobson, Protein Misfolding, functional amyloid and human disease, Annu. Rev. Biochem. 75 (2006) 333-366

[5] F. Chiti, C.M. Dobson, Protein misfolding, amyloid formation, and human disease: a summary of progress over the last decade, Annu. Rev. Biochem. 86 (2017) 27-68

[6] M. Perni, C. Galvagnion, A. Maltsev, G. Meisl, M.B.D. Müller, P.K. Challa, J.B. Kirkegaard, P. Flagmeier, S.I.A. Cohen, R. Cascella, S.W. Chen, R. Limbocker, P. Sormanni, G.T. Heller, F.A. Aprile, N. Cremades, C. Cecchi, F. Chiti, E.A.A. Nollen, T.P.J. Knowles, M. Vendruscolo, A. Bax, M. Zasloff, C.M. Dobson, A natural product inhibits the initiation of α-synuclein aggregation and suppresses its toxicity, PNAS 114(6) (2017) 1009-1017

[7] R. A. Hauser, D. Sutherland, J. A.Madrid, M. A. Rol, S.Frucht, S.Isaacson, F.Pagan, B.N.Maddux, G. Li, W. Tse, B. L. Walter, R. Kumar, D. Kremens, M. F.Lew, A. Ellenbogen, O.Oguh, A. Vasquez, W. Kinney, D. Barbut, Targeting neurons in the gastrointestinal tract to treat Parkinson's disease, Disorders, 1 (2019) 2-7

[8] M.N. Rao, A.E. Shinnar, L.A. Noecker, T.L. Chao, B. Feibush, B. Snyder, I. Sharkansky, A. Sarkahian, X. Zhang, S.R. Jones. W.A Kinney, M. Zasloff, Aminosterols from the dogfish shark Squalus acanthias. J Nat Prod. 63(5) (2000) 631-635

[9] M. Perni, P. Flagmeier, R. Limbocker, R. Cascella, F.A. Aprile, C. Galvagnion, G.T. Heller, G. Meisl, S.W. Chen, J.R. Kumita, P.K. Challa, J.B. Kirkegaard, S.I.A. Cohen, B. Mannini, D. Barbut, E.A.A. Nollen, C. Cecchi, N. Cremades, T.P.J. Knowles, F. Chiti, M. Zasloff, M. Vendruscolo, C.M. Dobson, Multistep inhibition of α-synuclein aggregation and toxicity in vitro and *in vivo* by trodusquemine, ACS Chem. Biol. 13(8) (2018) 2308–2319

[10]K.S. Moore, S.Wehrli, H.Roder, M. Rogers, J.N. Forrest, Jr D. McCrimmon,M. Zasloff,Squalamine: an aminosterol antibiotic from the shark, PNAS 90 (4) (1993) 1354-1358

[11] M. Zasloff, A. Paige Adams, B. Beckerman, A. Campbell, Z. Han, E. Luijten, I. Meza, J. Julander, A. Mishra, W. Qu, J.M. Taylor, S.C. Weaver, G.C.L. Wong, Squalamine as a broad-spectrum systemic antiviral agent with therapeutic potential, PNAS 108(38) (2011) 15978-15983

[12] M. Perni, C. Galvagnion, A. Maltsev, G. Meisl, M.B.D. Müller, P.K. Challa, J.B. Kirkegaard, P. Flagmeier, S.I.A. Cohen, R. Cascella, S.W. Chen, R. Limbocker, P. Sormanni, G.T. Heller, F.A. Aprile, N. Cremades, C. Cecchi, F. Chiti, E.A.A. Nollen, T.P.J. Knowles, M. Vendruscolo, A. Bax, M. Zasloff, C.M. Dobson, A natural product inhibits the initiation of α-synuclein aggregation and suppresses its toxicity, PNAS 114(6) (2017) 1009-1017

[13] R. A. Hauser, D. Sutherland, J. A.Madrid, M. A. Rol, S.Frucht, S.Isaacson, F.Pagan, B.N.Maddux, G. Li, W. Tse, B. L. Walter, R. Kumar, D. Kremens, M. F.Lew, A. Ellenbogen, O.Oguh, A. Vasquez, W. Kinney, D. Barbut, Targeting neurons in the gastrointestinal tract to treat Parkinson's disease, Disorders, 1 (2019) 2-7

[14]M.N. Rao, A.E. Shinnar, L.A. Noecker, T.L. Chao, B. Feibush, B. Snyder, I. Sharkansky, A. Sarkahian, X. Zhang, S.R. Jones. W.A Kinney, M. Zasloff, Aminosterols from the dogfish shark Squalus acanthias. J Nat Prod. 63(5) (2000) 631-635

[15] M. Perni, P. Flagmeier, R. Limbocker, R. Cascella, F.A. Aprile, C. Galvagnion, G.T. Heller, G. Meisl, S.W. Chen, J.R. Kumita, P.K. Challa, J.B. Kirkegaard, S.I.A. Cohen, B. Mannini, D. Barbut, E.A.A. Nollen, C. Cecchi, N. Cremades, T.P.J. Knowles, F. Chiti, M. Zasloff, M. Vendruscolo, C.M. Dobson, Multistep inhibition of α-synuclein aggregation and toxicity in vitro and *in vivo* by trodusquemine, ACS Chem. Biol. 13(8) (2018) 2308–2319

[16] R. Limbocker, S. Chia, F.S. Ruggeri, M. Perni, R. Cascella, G.T. Heller, G. Meisl, B. Mannini, J. Habchi, T.C.T. Michaels, P.K. Challa, M. Ahn, S.T. Casford, N. Fernando, C.K. Xu, N.D. Kloss, S.I.A. Cohen, J.R. Kumita, C. Cecchi, M. Zasloff, S. Linse, T.P.J. Knowles, F. Chiti, M. Vendruscolo, C.M. Dobson, Trodusquemine enhances $A\beta_{42}$ aggregation but suppresses its toxicity by displacing oligomers from cell membranes, Nat. Commun. 10 (2019) 225

[17] K.A. Lantz, S.G. Emeigh Hart, S.L Planey, M.F. Roitman, I.A. Ruiz-White, H.R. Wolfe, M.P. McLane, Inhibition of PTP1B by trodusquemine (MSI-1436) causes fat-specific weight loss in diet-induced obese mice, Obesity (Silver Spring) 18(8) (2010) 1516-1523

[18] A.M. Smith, K.K. Maguire-Nguyen, T.A. Rando, M.A. Zasloff, K.B. Strange, V.P. Yin, The protein tyrosine phosphatase 1B inhibitor MSI-1436 stimulates regeneration of heart and multiple other tissues, NPJ Regen. Med. 2(4) (2017).

[19] R. Limbocker, B. Mannini, F.S. Ruggeri, R. Cascella, C.K. Xu, M. Perni, S. Chia, S.W. Chen, J. Habchi, A. Bigi, R.P. Kreiser, A.K. Wright, J.A. Albright, T. Kartanas, J.R. Kumita, N. Cremades, M. Zasloff, C. Cecchi, T.P.J. Knowles, F. Chiti, M. Vendruscolo, C.M. Dobson, Trodusquemine displaces protein misfolded oligomers from cell membranes and abrogates their cytotoxicity through a generic mechanism, Commun. Biol. 3 (2020) 435

[20] S. Errico, G. Lucchesi, D. Odino, S. Muscat, C. Capitini, C. Bugelli, C. Canale, R. Ferrando, G. Grasso, D. Barbut, M. Calamai, A. Danani, M. Zasloff, A. Relini, G. Caminati, M. Vendruscolo, F. Chiti, Making

biological membrane resistant to the toxicity of misfoldedproteinoligomers: a lesson from trodusquemine, Nanoscale 12(44) (2020) 22596-22614
[21] G. Fragneto, R. Delhom, L. Joly, E. Scoppola, Neutrons and model membranes: Moving towards complexity, COCIS 38 (2018) 108-121
[22] G. Van Meer, D. Voelker, G. Feigenson, Membrane lipids: where they are and how they behave, Nat. Rev. Mol. Cell Biol. 9 (2008) 112–124
[23]H.I. Ingólfsson, M.N. Melo, F.J. van Eerden, C.Arnarez, C.A. Lopez, T.A. Wassenaar, X. Periole, A.H. de Vries, D.P. Tieleman, S.J. Marrink, Lipid organization of the plasma membrane, J. Am. Chem. Soc. 136(41) (2014) 14554-14559
[24]H.I. Ingólfsson, T.S. Carpenter, H. Bhatia, P.T. Bremer, S.J. Marrink, F.C. Lightstone, Computational Lipidomics of the Neuronal Plasma Membrane,Biophys. J. 113(10) (2017) 2271-2280
[25]T.K.M. Nyholm, D. Lindroos, B. Westerlund, J.PeterSlotte, Construction of a DOPC/PSM/Cholesterol Phase Diagram Based on the Fluorescence Properties of trans-Parinaric Acid, Langmuir 27(13) (2011) 8339–8350
[26] K. Simons, E. Ikonen, Functional rafts in cell membranes, Nature 387 (1997) 569-572
[27] R.G. Parton, A.A. Richards, Lipid rafts and caveolae as portals for endocytosis: new insights and common mechanisms, Traffic 4 (2003) 724-738
[28] K. Jacobson, O. Mouritsen, R. Anderson, Lipid rafts: at a crossroad between cell biology and physics, Nat. Cell Biol. 9 (2007) 7–14
[29] S. Rauch, O.T. Fackler, Viruses, lipid rafts and signal transduction, J. Signal Transduct. 7 (2007) 53-63
[30] J.V. Rushworth, N.M. Hooper, Lipid rafts: linking alzheimer's amyloid-β production, aggregation, and toxicity at neuronal membranes, Int. J. Alzheimer's Dis. 2011, Article ID 603052
[31] K.S. Vetrivel, G. Thinakaran, Membrane rafts in Alzheimer's disease beta-amyloid production, BBA - Mol. Cell. Biol. L. 1801 (2010) 860-867
[32]C. Galvagnion, The Role of Lipids Interacting with α-Synuclein in the Pathogenesis of Parkinson's Disease, J.Parkinsons Dis. 7(3) (2017) 433-450
[33] Y. Liu, J. Barnoud, S.J. Marrink, Gangliosides destabilize lipid phase separation in multicomponent membranes, Biophys. J. 117 (2019) 1215-1223
[34] C. Hao, L. Zhang, R. Sun, J. Yang, G. He, Interaction between ganglioside G_{M1} and diosgenin in langmuir monolayers at the air/water interface, Scanning 36 (2014) 218–223
[35] N. Yamamoto, Y. Fukata, M. Fukata, K. Yanagisawa, GM1-ganglioside-induced Abeta assembly on synaptic membranes of cultured neurons, BBA - Biomembranes 1768 (2007) 1128–1137
[36] W. Michno, P.M. Wehrli, H. Zetterberg, K. Blennow, J. Hanrieder, GM1 locates to mature amyloid structures implicating a prominent role forglycolipid-protein interactions in Alzheimer pathology, BBA - Proteins and Proteomics 1867 (2019) 458–467
[37]T.K.M. Nyholm, D. Lindroos, B. Westerlund, J.P. Slotte, Construction of a DOPC/PSM/Cholesterol Phase Diagram Based on the Fluorescence Properties of trans-Parinaric Acid, Langmuir 27(13) (2011) 8339–8350
[38] G.L. Gaines, Insoluble monolayers at liquid-gas interfaces, Interscience Publishers, New York (1966)
[39] P. Wydro, The magnitude of condensation induced by cholesterol on the mixtures of sphingomyelin with phosphatidylcholines-Study on ternary and quaternary systems, Colloids Surf. B 82 (2011) 594-601
[40] P. Wydro, Sphingomyelin/phosphatidylcholine/cholesterol monolayers - analysis of the interactions in model membranes and Brewster Angle Microscopy experiments, Colloids Surf. B 93 (2012) 174–179
[41] M. Jurak, M. Golabek, L. Holysz, E. Chibowski, Properties of Langmuir and solid supported lipid films with sphingomyelin, Adv. Colloid Interface Sci. 222 (2015) 385–397
[42] K.S Birdi, Lipid and biopolymer monolayers at liquid interfaces, Plenum Press, New York (1989)
[43] M.N. Jones, D. Chapman, Micelles, monolayers and biomembranes, Wiley–Liss, New York and Chichester (1995)
[44] J.T. Davies, E.K. Rideal, Interfacial Phenomena, Academic Press, New York (1963)
[45] D.J. Crisp, Surface Chemistry, Butterworths, London (1949)

[46] G. Caminati, G. Gabrielli, M. Puggelli, E. Ferroni, Mixed monolayers of polymethacrylic esters containing aromatic and aliphatic groups, Colloid Polym. Sci. 267(3) (1989) 237-245
[47] T-H. Chou, I-M. Chu, C.-H. Chang, Interaction of paclitaxel with DSPC in monolayers at the air/water interface at different temperatures, Colloids Surf. B 25 (2002) 147–155
[48] J.M. Pusterla, A.A. Malfatti-Gasperini, X.E. Puentes-Martinez, L.P. Cavalcanti, R.G. Oliveira, Refractive index and thickness determination in Langmuir monolayers of myelin lipids, BBA - Biomembranes 1859 (2017) 924–930
[49] I. Budziak, M. Arczewska, M. Sachadyn-Król, A. Matwijczuk, A. Waśko, M. Gagoś, K. Terpiłowski, D.M. Kamiński, Effect of polyols on the DMPC lipid monolayers and bilayers, BBA - Biomembranes 1860 (2018) 2166–2174
[50] T.A Wassenaar, H.I. Ingólfsson, R.A. Böckmann, D.P. Tieleman, S.J. Marrink, Computational Lipidomics with insane: A Versatile Tool for Generating Custom Membranes for Molecular Simulations, J. Chem. Theory Comput. 11 (2015) 2144–2155
[51] G. Bussi, D. Donadio, M. Parrinello, Canonical sampling through velocity rescaling. J. Chem. Phys. 126 (2007) 014101
[52] H.J.C. Berendsen, J.P.M. Postma, W.F. van Gunsteren, A. DiNola, J.R. Haak, Molecular dynamics with coupling to an external bath, J. Chem. Phys. 81 (1984) 3684–3690
[53] S. Thallmair, M. Javanainen, B. Fábián, H. Martinez-Seara, S.J. Marrink, Nonconverged Constraints Cause Artificial Temperature Gradients in Lipid Bilayer Simulations. J. Phys. Chem. B 125(33) (2021) 9537-9546
[54] M. Parrinello, A. Rahman, Polymorphic transitions in single crystals: A new molecular dynamics method. J. Appl. Phys. 52 (1981) 7182–7190
[55] T. Darden, D. York, L. Pedersen, Particle mesh Ewald: An N·log(N) method for Ewald sums in large systems. J. Chem. Phys. 98 (1993) 10089–10092
[56] S.J. Marrink, H.J. Risselada, S. Yefimov, D.P. Tieleman, A.H. de Vries, The MARTINI Force Field: Coarse Grained Model for Biomolecular Simulations The MARTINI Force Field: Coarse Grained Model for Biomolecular Simulations. J. Phys. Chem. B 111(27) (2007) 7812–7824
[57] M.J. Abraham, T. Murtola, R. Schulz, S. Páll, J.C. Smith, B. Hess, E. Lindhl, Gromacs: High performance molecular simulations through multi-level parallelism from laptops to supercomputers. SoftwareX 1–2 (2015) 19–25
[58] R.E. Brown, H.L. Brockman, Using monomolecular films to characterize lipid lateral interactions, Methods Mol. Biol. 398 (2007) 41-58
[59] D. Vaknin, M.S. Kelley, B.M. Ocko, Sphingomyelin at the air–water interface, J. Chem. Phys. 115 (2001) 7697-7704
[60] K. Hąc-Wydro, P. Dynarowicz-Łątka, The impact of sterol structure on the interactions with sphingomyelin in mixed langmuir monolayers, J. Phys. Chem. B 112(36) (2008) 11324-11332
[61] C-C. Hao, R-G. Sun, J. Zhang, Interaction of egg-sphingomyelin with dopc in langmuir monolayers, Chinese J. Chem. Phys. 25 (2012) 691-696
[62] R. Volinsky, R. Paananen, P.K.J. Kinnunen, Oxidized phosphatidylcholines promote phase separation of cholesterol-sphingomyelin domains, Biophys. J. 103(2) (2012) 247-254
[63] F.T. Presti, The role of cholesterol in regulating membrane fluidity, Membrane Fluidity in Biology, Academic Press (1985) 97–146
[64] J.R. Silvius, (2003). Role of cholesterol in lipid raft formation: lessons from lipid model systems, BBA - Biomembranes 1610(2) (2003) 174–183
[65] R.A. Demel, W.S.M. Guerts van Kessel, L.L.M. van Deenen, The properties of polyunsaturated lecithins in monolayers and liposomes and the interactions of these lecithins with cholesterol, BBA - Biomembranes, 266(1) (1972) 26-40

[66] J.M. Smaby, H.L. Brockman, R.E. Brown, Cholesterol's interfacial interactions with sphingomyelins and phosphatidylcolines: hydrocarbon chain structure determines the magnitude of condensation, Biochemistry, 33 (1994) 9135-9142
[67] T.G. Anderson, H.M. McConnell, Condensed complexes and the calorimetry of cholesterol-phospholipid bilayers, Biophys. J. 81 (2001) 2774-2785
[68] E. London, Insights into lipid raft structure and formation from experiments in model membranes, Curr. Op. Struc. Biol. 12 (2002) 480-486
[69] R.F.M. de Almeida, A. Fedorov, M. Prieto, Sphingomyelin/phosphatidylcholine/cholesterol phasediagram: boundaries and composition of lipid rafts, Biophys J. 85 (2003) 2406–2416
[70] A. Bunge, P. Muller, M. Stockl, A. Herrmann, D. Huster, Characterization of the ternary mixture of sphingomyelin, POPC, and cholesterol: support for an inhomogeneous lipid distribution at high temperatures, Biophys. J. 94 (2008) 2680–2690
[71] P. Dynarowicz-Latka, K. Hac-Wydro, Interactions between phosphatidylcholines and cholesterol in monolayers at the air/water interface, Colloids Surf. B 37 (2004) 21–25
[72] K. Hac-Wydro, P. Wydro, P. Dynarowicz-Latka, M. Paluch, Cholesterol and phytosterols effect on sphingomyelin/phosphatidylcholine model membranes — thermodynamic analysis of the interactions in ternary monolayers, J. Colloid Interface Sci.329 (2009) 265–272
[73] L.K. Tamm, H.M. McConnell, Supported phospholipids bilayers, Biophys. J. 47 (1985) 105–13
[74] E. Chibowski, M. Jurak, L. Holysz, Preparation, investigation techniques and surface free energy of solid supported phospholopid layers. The encyclopedia of surface and colloid science. 2nd ed. Taylor & Francis Group (2012) 1–22
[75]I.Basu, C. Mukhopadhyay, In silico phase separation in the presence of GM1in ternary and quaternary lipid bilayers, Phys.Chem.Chem.Phys., 17 (2015) 17130-17139
[76] T. Benvegnu, L. Lemiegre, S. Cammas-Marion, Archaeal lipids: innovative materials for biotechnological applications. Eur. J. Org. Chem. 28 (2008) 4725–4744
[77] F. Hentrich, C. Tschierske, H. Zaschke, BolaamphiphilePolyole, eine neue Klasse amphotroper Flüssigkristalle, Angew. Chem. 103(4) (1991) 429 – 431
[78] J.H. Fuhrhop, T. Wang, Bolaamphiphiles Chem. Rev. 104(6) (2004) 2901 – 2937
[79] Z. Huang, Y.M. Zhang, Q. Cheng, J. Zhang, Y.H. Liu, B. Wang, X.Q. Yu, Structure-activity relationship studies of symmetrical cationic bolasomes as non-viral gene vectors, J. Mater. Chem. B 4 (2016) 5575–5584
[80] B. Mecheria, F. Gambinossi, M. Nocentini, M. Puggelli, G. Caminati, Modulation of tetracycline–phospholipid interactions by tuning of pH at the water–air interface, Biophys. Chem. 111 (2004) 15– 26
[81] S.P. Moulik, A.K. Rakshit, B. Naskar, Evaluation of non-ambiguous critical micelle concentration of surfactants in relation to solution behavior of pure and mixed surfactant systems: a physicochemical documentary and analysis, J. Surfactant and deterg. 24 (2021) 535-549
[82] G. Roberts, Langmuir-Blodgett Films, Plenum Press, New York (1990)
[83] A.P. Patwardhan, D.H. Thompson, Novel flexible and rigid tetraether acyclic and macrocyclic bisphosphocholines: synthesis and monolayer properties, Langmuir 16(26) (2000) 10340–10350
[84] N. Mizoshita, T. Seki, Flat orientation of hydrophobic cores induced by two-dimensional confinement of flexible bolaamphiphiles at the air−water interface, Langmuir 21(23) (2005) 10324–10327
[85] P. Niton, A. Zywocinski, J. Paczesny, M.Fiałkowski, R. Hołyst, B. Glettner, R. Kieffer, C. Tschierske, D. Pociecha, E. Gorecka Aggregation and layering transitions in thin films of X-, T-, and anchor-shaped bolaamphiphiles at the air–water interface, Chem. Eur. J. 17 (2011) 5861 – 5873
[86] A. Meister, M.J. Weygand, G. Brezesinski, A. Kerth, S. Drescher, B. Dobner, A. Blume, Evidence for a reverse U-shaped conformation of single-chain bolaamphiphiles at the air-water jnterface, Langmuir 23 (2007) 6063-6069
[87] B. Glettner, F. Liu, X.B. Zeng, M. Prehm, U. Baumeister, G. Ungar, C. Tschierske, Liquid-crystal engineering with anchor-shaped molecules: honeycombs with hexagonal and trigonal symmetries formed by polyphilic bent-core molecules, Angew. Chem. Int. Ed. 47(32) (2008) 6080 – 6083

[88] R.M. Lamarche, C. DeWolf, ω-Thiolation of phenolic surfactants enables controlled conversion between extended, bolaform, and multilayer conformations, Langmuir 36(11) (2020) 2847–2857

[89] F.A. Heberle, R.S. Petruzielo, J. Pan, P. Drazba, N. Kučerka, R.F. Standaert, G.W. Feigenson, J. Katsaras, Bilayer thickness mismatch controls domain size in model membrane's J. Am. Chem. Soc. 135(18) (2013) 6853-6859

[90]B.L.Stottrupa, A.H.Nguyena, E. Tüzelb, Taking another look with fluorescence microscopy: Image processing techniques in Langmuir monolayers for the twenty-first century, Biochim.Biophys. Acta (BBA) – Biomembranes 1798(7) (2010) 1289-1300

[91]I. Sriram, B.Singhana, T.R. Lee, D.K. Schwartz, Line Tension and Line Activity in Mixed Monolayers Composed of Aliphatic and Terphenyl-Containing Surfactants, Langmuir 28(47) (2012) 16294–16299

[92] A.J. García-Sáez, S. Chiantia, P. Schwille, Effect of Line Tension on the Lateral Organization of Lipid Membranes, J. Biol.Chem. 282(46) (2007) 33537 - 33544

[93] Z. Pernber, K. Blennow, N. Bogdanovic, J.-E. Mensson, M. Blomqvist, Altered Distribution of the Gangliosides GM1 and GM2 in Alzheimer's Disease, Dement. Geriatr. Cogn. Disord. 33 (2012) 174–188

[94] R. Cascella, E. Evangelisti, A. Bigi, M. Becatti, C. Fiorillo,M. Stefani, F. Chiti and C. Cecchi, Soluble Oligomers Require a Ganglioside to Trigger Neuronal Calcium Overload, Journal of Alzheimer's Disease 60 (2017) 923–938

[95] Y. Ohta, S. Yokoyama, H. Sakai, M. Abe, Membrane properties of binary and ternary systems of ganglioside GM1/dipalmitoylphosphatidylcholine/dioleoylphosphatidylcholine, Colloids Surf. B 34(3) (2004) 147-153

[96] H. Juhola, P.A. Postila, S. Rissanen, F. Lolicato, I. Vattulainen, T. Róg, Negatively charged gangliosides promote membrane association of amphipathic neurotransmitters, Neuroscience 384 (2018) 214–223

[97] E. Evangelisti, D. Wright, M. Zampagni, R. Cascella, C. Fiorillo, S. Bagnoli, A. Relini, D. Nichino, T. Scartabelli, B. Nacmias, S. Sorbi, C. Cecchi, Lipid rafts mediate amyloid-induced calcium dyshomeostasis and oxidative stress in Alzheimer's disease, Curr Alzheimer Res. 10(2) (2013) 143-53.

[98] T-Pham, K. H. Cheng, Exploring the binding kinetics and behaviors of self-aggregated beta-amyloid oligomers to phase-separated lipid rafts with or without ganglioside-clusters, Biophysical Chemistry 290 (2022) 106874

[99] *T.* Kawarabayashi, T. Nakamura, K. Sato, Y. Seino, S. Ichii, N. Nakahata, M.Takatama, D. Westaway, P. George-Hyslop, M.Shoji, Lipid Rafts Act as a Common Platform for Amyloid-β Oligomer-Induced Alzheimer's Disease Pathology Journal of Alzheimer's Disease, 87(3) (2022) 1189-1203